Design of a Transition-Edge Hot-Electron Microbolometer for Millimeter-Wave Astrophysical Observations

Emily M. Barrentine, Shafinaz Ali, Christine A. Allen, Ari D. Brown, Nga T. Cao, James A. Chervenak, Kevin L. Denis, Wen-Ting Hsieh, Timothy M. Miller, S. Harvey Moseley, Thomas R. Stevenson, Peter T. Timbie, Douglas E. Travers, Kongpop U-Yen, and Edward J. Wollack

***Abstract*—We are developing a Transition-edge Hot-electron Microbolometer (THM) with the capacity to make sensitive and broadband astrophysical observations over frequencies ranging from 30–300 GHz (10-1 mm). This micron-sized bolometer consists of a superconducting bilayer Transition-Edge Sensor (TES) and a thin-film absorber. The THM employs the decoupling between electrons and phonons at low temperatures (below 300 mK) to provide thermal isolation. The devices are fabricated photolithographically and read out with Superconducting Quantum Interference Devices (SQUIDs). We present the details of a thermal model for a THM detector and the design for new thermally optimized antenna-coupled THMs for illumination by a RF source at 40 and 100 GHz.**

***Index Terms*—Bolometers, hot-electron, millimeter wave detectors, superconducting sensors.**

I. Introduction

ASTROPHYSICAL measurements at millimeter wavelengths now require arrays of photon-noise-limited detectors for both broad-band and narrow-band applications. In particular, future measurements of the Cosmic Microwave Background (CMB), including the observation of B-mode polarization to detect the imprint of gravitational waves from inflation, will require an order of magnitude increase in CMB detector sensitivity [1]. Presently, individual CMB detectors have reached photon-noise-limited levels, and further advances will require arrays of 1000 s of detectors. Low noise arrays are also required for millimeter-wave spectroscopy [2]. One of the most promising technologies for application to millimeter-wave detector arrays are cryogenic TES bolometric detectors read out by low power, low noise, multiplexed SQUIDs [3]. These TES detectors make use of the sharp transitional properties of superconductors to measure the temperature dependence of an RF absorbing bolometer. They can be voltage-biased to keep the TES in the sensitive transition region via electrothermal feedback due to Joule power dissipation in the TES [4], [5].

Bolometric detectors directly absorb incident radiation thermally. An important component to the operation of these bolometers is the thermal link between the detector and a cold bath. Common TES bolometers make use of micro-machined isolation structures, first introduced by Downey *et al.*, [6], to precisely control the thermal conductance of the link. This thermal conductance affects the noise, time response, saturation level and bias point of the detector. These membrane structures are fragile and present both fabrication and design complexities, especially when the technique is extended to large arrays.

The Transition-Edge Hot-Electron Microbolometer (THM) makes use of a different type of thermal isolation, one that is controlled by the weak coupling between electrons and phonons in the detector at low temperatures. This hot-electron design is similar to a design by Wei *et al.* [7], but contains a separate absorbing structure. The advantages of this thermal design are easy and robust fabrication, a small cross-sectional area for cosmic rays and close packing into the focal plane, a short thermal time constant, low thermal conductance, and separate impedance matching of the absorber to the transmission lines.

II. Thermal Model

The basic design of the THM consists of a metal Bi absorber overlapping a superconducting bilayer Au/Mo TES. The absorber terminates a Nb superconducting microstrip transmission line. The detector is operated at milliKelvin temperatures to increase sensitivity.

The heat flow within the detector is controlled by electron-electron scattering between the electrons in the TES and absorber and electron-phonon scattering between the electrons and the phonons in the detector. Andreev reflection of the electrons in the detector at the superconducting Nb transmission lines keeps heat from dissipating out the leads [8]. The Kapitza boundary resistance between the detector and substrate phonons is minimal due to the thinness of the metal film relative to phonon wavelength [9]. A thermal model of the detector is show in Fig. 1.

The thermal conductance for electron-electron scattering follows $G_{e-e} = L_0 T_c / R$ [10]. Here R is the electrical resistance of the detector, L_0 is the Lorentz constant, where $L_0 =$

Manuscript received August 25, 2008. First published June 30, 2009; current version published July 10, 2009. This work was supported in part by the NASA Graduate Student Researcher Program.

E. M. Barrentine and P. T. Timbie are with the University of Wisconsin-Madison, Madison, WI 53706 USA (e-mail: barrentine@wisc.edu).

S. Ali is with Merritt College, Oakland, CA 94619 USA.

C. A. Allen, A. D. Brown, N. T. Cao, J. A. Chervenak, K. L. Denis, W. T. Hsieh, T. M. Miller, S. H. Moseley, T. R. Stevenson, D. E. Travers, K. U-Yen and E. J. Wollack are with the NASA-Goddard Space Flight Center, Greenbelt, MD 20771 USA.

Color versions of one or more of the figures in this paper are available online at http://ieeexplore.ieee.org.

Digital Object Identifier 10.1109/TASC.2009.2017956

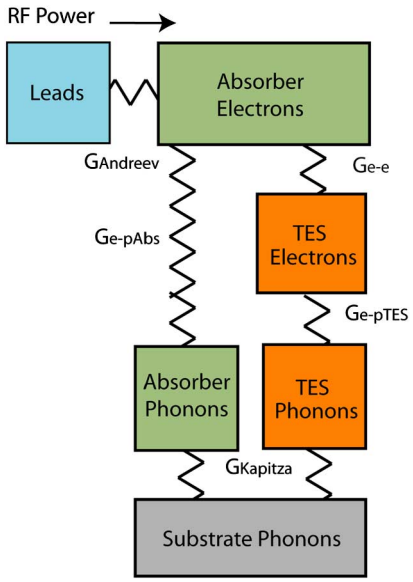

Fig. 1. The thermal model of the THM detector.

2.44×10^{-8} W $\cdot\ \Omega/\mathrm{K}^2$, and T_c is the operating temperature of the detector. The thermal conductance for electron-phonon scattering is given by $G_{e-p} = 5V\Sigma T_c^4$ where V is the volume of the detector, and Σ is a material dependent constant [9]. The electron-phonon thermal conductance for the entire detector is then given by $G_{e-p} = G_{e-pAbs} + G_{e-pTES}$. Here G_{e-pAbs} and G_{e-pTES} are the respective electron-phonon conductances of the Bi absorber and the Au TES and depend on their respective volumes, V_{Abs} and V_{TES}.

We have tested prototype THM devices, measuring noise, responsivity and thermal conductance, to confirm the electron-phonon Σ values for a Au/Mo TES and Bi/Au absorber [11], [12]. These values agree with literature Σ values for Au and Bi [13], [14]. They are also consistent with the T_c^4 temperature dependence of G_{e-p}.

III. Optimization of Thermal Model

To achieve photon-noise limited levels the noise-equivalent power of the detector, $NEP_{DETECTOR}$, must be less than NEP_{PHOTON}, the unavoidable statistical fluctuation noise due to variation in the arrival rate of photons at the detector [15], [16]. In Table I, NEP_{PHOTON} is calculated for both ground and space-based applications for a single ideal bolometric detector observing a blackbody sky with temperature T_{sky} in the Raleigh-Jeans limit.

$NEP_{DETECTOR}$ contributions include noise from thermal fluctuations across the thermal link between the detector and cold reservoir $(NEP_{THERMAL})$, Johnson noise fluctuations $(NEP_{JOHNSON})$ across the biased resistive TES and within the bias circuit, and amplifier noise from the SQUID readouts (NEP_{SQUID}).

$NEP_{THERMAL}$ for the case an ideal electron-phonon dominated detector is given by

$$NEP_{thermal} = \sqrt{2k_B G(T_{bath}) T_{bath}^2 \left[\frac{T_c^6}{T_{bath}^6} + 1\right]}$$

TABLE I
THM Optimization

Observing and Detector Parameters	Ground Observing	Space Observing
Center Frequency	100 GHz	100 GHz
Bandwidth	20 GHz	20 GHz
# of modes	1	1
Optical Efficiency	50%	50%
T_{bath}	240 mK	100 mK
T_{sky}	250 K	2.7 K
Sky emmisivity	0.04	1.0
NEP_{PHOTON}	2×10^{-17} W/√Hz	5×10^{-18} W/√Hz
Incident Power from Sky	4×10^{-12} W	4×10^{-13} W
TES Bias Power	1×10^{-11} W	1×10^{-12} W
Microstrip Impedance	20 Ω	20 Ω
Bismuth Resistivity at 4K	2600 uΩ·cm	2600 uΩ·cm
Σ_{Bi}	2.4×10^8	2.4×10^8
Σ_{Au}	4.2×10^9	4.2×10^9
Au TES Thickness	350 nm	350 nm
Bi Absorber Thickness	1200 nm	1200 nm
Absorber Area	3 μm x 6 μm	3 μm x 6 μm
TES Area	3 μm x 3 μm	3 μm x 3 μm
T_c	270 mK	150 mK
$G_{e\text{-}p}$	5×10^{-10} W/K	5×10^{-11} W/K
$G_{e\text{-}pAbs}$	7×10^{-11} W/K	7×10^{-12} W/K
$G_{e\text{-}e}$	3×10^{-10} W/K	2×10^{-10} W/K
$NEP_{THERMAL}$	4×10^{-17} W/√Hz	6×10^{-18} W/√Hz
$NEP_{JOHNSON}$	1×10^{-17} W//√Hz	3×10^{-18} W//√Hz
$NEP_{DETECTOR}$	4×10^{-17} W/√Hz	7×10^{-18} W/√Hz
Heat Capacity, C	6×10^{-17} J/K	4×10^{-17} J/K
Thermal Time Constant	<0.1 μs	<0.7 μs

The input parameters and results of the THM optimization scheme. The only design difference between ground and space application is a lower bath temperature. The low heat capacity of the devices leads to very fast detectors, with thermal time constants less than 1 μs with electrothermal feedback. For Johnson noise calculations we have assumed $\alpha = 200$, $\beta = 0$, $R_{SHUNT} = 25\ \mathrm{m}\Omega$, and $R_{TES} = 0.1\ \Omega$. We expect NEP_{SQUID} to occur well below the photon-noise limit.

[17], [18]. Here T_{bath} is the temperature of the cold bath. Minimizing $NEP_{THERMAL}$ requires minimizing the bath and detector operating temperatures, as well as the thermal conductance of the bolometer. For an electron-phonon dominated detector this requires minimizing the detector volume.

It is necessary to point out that if the detector thermal conductance is made too low, the thermal noise actually increases, due to the increase in bolometer temperature for a given power load. In our case, fabrication constraints on the volume of the detector limit the thermal conductance and NEP before this stage. It is also important to note that in the case where the electrons in the detector are not in thermal equilibrium, when $G_{e-pAbs} > G_{e-e}$, additional thermal noise fluctuations arise. Such a situation also allows incident power to bypass the TES, leading to a reduction in sensitivity.

The Johnson noise of the detector depends on the TES resistance, R_{TES}, the transition behavior of the TES characterized by $\alpha = (T_c/R_{TES})(dR_{TES}/dT_c)$ and $\beta = (I_{TES}/R_{TES})(dR_{TES}/dI_{TES})$, as well as the bias conditions. Here I_{TES} is the current through the voltage-biased TES which is read out by the SQUID. Applying the matrix method developed by Lindeman [19], [20] we have calculated the Johnson noise of an ideal bolometer in the linear regime for this optimized design. These estimates are shown Table I

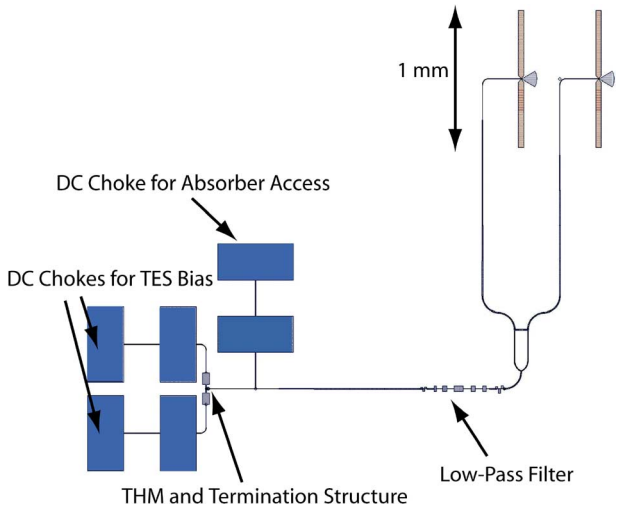

Fig. 2. Microwave design at 92 GHz to couple radiation to the optimized THM detector. The signal from the double slot antenna is transmitted via a low pass filter to the RF terminated THM detector. DC choked bias leads provide access to both the TES and absorber. The absorber access will allow us to apply a DC bias to dissipate Joule power in the absorber in order to measure thermal conductance and compare DC to RF response.

and assumes a bias circuit with a shunt resistor, R_{SHUNT}, in parallel with the TES read out by a SQUID with input coil inductance, $L = 10$ nH.

A THM optimization scheme thus requires both $G_{e-pAbs} < G_{e-e}$ and $NEP_{DETECTOR} \leq NEP_{PHOTON}$. We have applied this optimization to the basic THM design, taking into account reasonable fabrication constraints for film thicknesses and line widths and requiring an absorber resistance, $R_{ABS} = 20\ \Omega/\text{square}$, to impedance match to the microstrip transmission lines. The resulting design from this optimization scheme is a $3\ \mu\text{m} \times 3\ \mu\text{m}$ square Mo/Au TES overlapped by a $6\ \mu\text{m} \times 3\ \mu\text{m}$ Bi absorber, whose properties are shown in Table I. This detector size is near the fabrication limit for standard photolithography.

IV. Test Devices & Microwave Design

These new optimized THM test devices were recently fabricated at NASA Goddard Detector Development Laboratory. These test devices have a target transition temperature of 250 mK. The devices are designed to couple to an RF signal transmitted via a 3 μm wide, 20 Ω, $\text{Nb}/\text{Al}_2\text{0}_3/\text{Nb}$ microstrip transmission line. This transmission line is coupled to a double-slot antenna (see Fig. 2) based upon a similar design by Zmuidzinas and LeDuc [21]. The microwave circuit includes a low-pass filter to eliminate spurious high frequency passbands from the antenna. The devices are designed to operate at 43 or 92 GHz.

The small area of the absorber requires that the incoming RF radiation be absorbed over a short distance compared to the effective wavelength of the radiation. To complete this termination a Nb microstrip termination structure is used, shown in Fig. 3. This structure creates an absorbing resonance at the center frequency of the circuit. A simulation of this absorption is shown in Fig. 4.

We have fabricated many variations of the microwave design in order to characterize individual microwave elements. Most importantly, the slot antenna will provide coupling to a swept or blackbody RF source to test the RF response of the THM detectors.

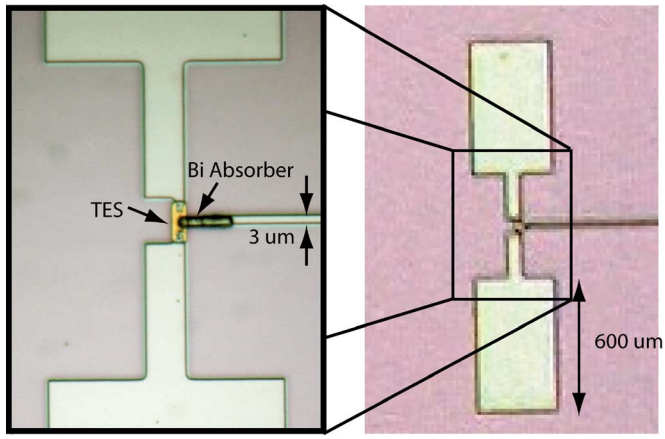

Fig. 3. On left, the optical image of one of the optimized THM test devices. The incident signal (transmitted from the right) terminates on the 1200 nm Bi absorber, which overlaps the 65 nm Mo/350 nm Au TES. The termination structure, shown in whole in the larger perspective on the right, provides absorption over a very wide band.

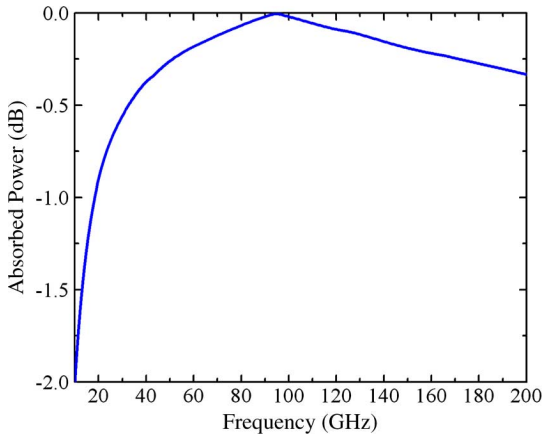

Fig. 4. A SONNET simulation of the THM termination structure for the THM coupled design at 92 GHz. Shown is the detector-absorbed power, for an RF signal inserted into transmission line at the base of absorber. The simulation predicts an extremely broadband termination. This simulation assumes an exact impedance match between the 20 Ω microstrip line and the 20 Ω Bi absorber. However, even a large mismatch in absorber resistance will result in minimal loss to reflection. An absorber resistance of 30 Ohms or 10 Ohms terminating a 20 Ohm microstrip will result in a 3% or 11% loss, respectively, of the incoming power to reflection.

V. Conclusion

To characterize the new optimized THM devices both DC and RF measurements are expected. These measurements will include resistance versus temperature, current-voltage (I-V), noise, responsivity and thermal conductance measurements. We also plan to complete RF tests of the microwave components, including the termination structure. We will use a variable 4–20 K blackbody located inside the dewar to couple RF radiation to the detectors and simulate CMB loading conditions.

Acknowledgment

The authors thank all those at the NASA Goddard Space Flight Center Detector Development Laboratory for their assis-

tance during the fabrication of these devices. EB would also like to thank Mark Lindeman and Dan McCammon for helpful discussions.

REFERENCES

[1] W. Hu and S. Dodelson, "Cosmics microwave background anisotropies," *Annu. Rev. Astron. and Astrophys.*, vol. 40, pp. 171–216, Sept. 2002.

[2] H. Nguyen *et al.*, "Z-spec's first light at the Caltech submillimeter observatory," *Nucl. Instrum. Methods Phys. Res. A.*, vol. 559, pp. 626–638, April 2006.

[3] Task Force on CMB Research, TFCR Final Report July 2005 [Online]. Available: http://www.nsf.gov/mps/ast/tfcr.jsp

[4] K. D. Irwin, "An application of electrothermal feedback for high resolution cryogenic particle detection," *Appl. Phys. Lett.*, vol. 66, pp. 1998–2000, April 1995.

[5] A. T. Lee, P. L. Richards, S. W. Nam, B. Cabrera, and K. D. Irwin, "A superconducting bolometer with strong electrothermal feedback," *Appl. Phys. Lett.*, vol. 69, pp. 1801–1803, Sept. 1996.

[6] P. M. Downey *et al.*, "Monolithic silicon bolometers," *Appl. Opt.*, vol. 23, pp. 910–914, March 1984.

[7] J. Wei *et al.*, "Ultrasensitive hot-electron nanobolometers for terahertz astrophysics," *Nature Nanotech.*, vol. 3, pp. 496–500, Aug. 2008.

[8] A. F. Andreev, "Thermal conductivity of the intermediate state of superconductors," *Sov. Phys. JETP*, vol. 19, p. 1228, Nov. 1964.

[9] F. C. Wellstood, C. Urbina, and J. Clarke, "Hot electron effect in metals," *Phys. Rev. B*, vol. 49, pp. 5942–5955, March 1994.

[10] F. Pobell, *Matter and Methods at Low Temperature*, 2nd ed. Berlin-Heidelberg: Springer, 1996.

[11] S. Ali *et al.*, "Antenna-coupled transition-edge hot-electron micro-bolometers," in *Proc. SPIE—Int. Soc. Opt. Eng.*, June 2004, vol. 5498, pp. 381–389.

[12] E. M. Barrentine *et al.*, "Sensitivity measurements of a transition-edge hot-electron microbolometer for millimeter-wave astrophysical observations," *J. Low Temp. Phys.*, vol. 141, pp. 173–179, April 2008.

[13] F. Pierre *et al.*, "Dephasing of electrons in mesoscopic metal wires," *Phys. Rev. B*, vol. 68, p. 085413, Aug. 2003.

[14] S. I. Dorozhkin, F. Lell, and W. Schoepe, "Energy relaxation of hot electrons and inelastic collision time in thin metal films at low temperatures," *Solid State Commun.*, vol. 60, pp. 245–248, 1986.

[15] P. L. Richards, "Bolometers for infared and millimeter waves," *J. Appi. Phys.*, vol. 76, pp. 1–24, July 1994.

[16] J. Zmuidzinas, "Thermal noise and correlations in photon detector," *Appl. Opt.*, vol. 42, pp. 4989–5008, Sept. 2003.

[17] W. S. Boyle and K. F. Rodgers, "Performance characteristics of a new low-temperature bolometer," *J. Opt. Soc. Am.*, vol. 49, pp. 66–69, Jan. 1959.

[18] D. McCammon, "Thermal equilibrium calorimeters—An introduction," in *Cryogenic Particle Detection*, C. Enss, Ed. Berlin Heidelberg: Springer-Verlag, 2005, ch. 1.

[19] M. Lindeman, "Microcalorimetery and the Transition-Edge Sensor," Ph.D. thesis, Dept. Appl. Sci., Univ. Calif. Davis., , 2000.

[20] E. Figueroa-Feliciano, "Theory and Development of Position-Sensitive Quantum Calorimeters," Ph.D. Thesis, Dept. of Phys., Stanford University, , 2001.

[21] J. Zmuidzinas and H. G. LeDuc, "Quasi-optical slot antenna SIS mixers," *IEEE Trans. Microwave Theory Tech.*, vol. 40, pp. 1797–1804, Sept. 1992.